Group Project Report

Bachelor of
Space Science and Satellite Technology

Impacts of Supermassive Black Hole Feedback on Galaxy Formation in IllustrisTNG Simulations

Project by

Nguyen Thi Yen Binh
Trinh Hoang Dieu Ngan
Nguyen Phu Huy
Huynh Quoc Thang

Supervisor: Dr. Truong Xuan Nhut
NASA Goddard Space Flight Center, University of Maryland in Baltimore County

University of Science and Technology of Hanoi
Hanoi, Vietnam

January 29, 2024

Contents

List of Figures

List of Tables

1 Introduction

Supermassive black holes (SMBH), those with a mass of millions of solar masses or greater, typically reside at the center of most galaxies in the local Universe (Kormendy & Ho 2013; Saglia et al. 2016). SMBHs are thought to be the central engines powering the feedback from the Active Galactic Nuclei (AGN) resulting from matter accreting onto the SMBH. Accreting SMBHs can release a substantial amount of energy ($\sim 10^{20}$ erg/s per gram of accreted matter) into their host galaxies. Consequently, they are anticipated to have profound impacts on the formation and evolution of galaxies. In this regard, SMBH feedback is considered as a fundamental ingredient in modern cosmological simulations of galaxy formation (see e.g Vogelsberger et al. 2019 for a review).

In this project, we aim to study the impacts of SMBH feedback on the galaxy formation and evolution by utilizing the IllustrisTNG Simulations (TNG hereafter, see Section 3.1 for a detailed description). TNG consists of cosmological magnetohydrodynamical simulations, which aim to model the evolution of matters in the Universe across the cosmic time. Within the TNG framework, numerous studies have proven the crucial role of SMBH feedback in reproducing realistic samples of galaxies both in terms of both stellar and gaseous components (e.g., Pillepich et al. 2019; Truong 2020; Ayromlou et al. 2023). Our aim is to conduct a comprehensive analysis of these effects on a variety of galaxy properties, thereby obtaining an overall picture of SMBH feedback activities in TNG simulations.

Particularly, we will explore the impacts of SMBH feedback on the star formation rate (SFR) as well as the specific star formation rate (sSFR), the baryon mass fraction contributed by both the gas and stellar components, the temperature of gaseous haloes, and the relationship between SMBH and halo mass.

The first part of the report provides a brief introduction to the project. Next, section 2 lays out a short summary of the theoretical background of galaxy formation. The third part details the materials as well as the scientific methods we used in order to carry out the project. Section 4 presents the results, with discussions on the results featured in. Then, we will conclude on what we have achieved throughout the project in section 6. Ultimately, section 7 shows the management of the project.

2 Theoretical Background

2.1 Galaxy Formation

Galaxies are gravitationally bound systems with dark matter halo as the backbone for structure formation. Each galaxy harbors a great number of stars, interstellar matter like gas and dust, stellar remnants like neutron stars and black holes.

In the early stages of the expanding Universe, the dynamics are primarily governed by dark matter (DM). Ultimately, the collapsing cloud attains virialization and comes to a standstill. Gas, in contrast to collisionless DM, has the capacity to cool and fragment on smaller scales (Chiaki et al. 2016). It condenses at the center of more extensive DM halos, and the denser regions further collapse to nurture the star formation. At the central core, SMBHs form, and they grow via accretion and mergers with other SMBHs. In return, Accreting SMBHs, i.e. AGN, can release feedback energy into their host galaxy.

Feedback from supernovae and active galactic nuclei, in the form of thermal and kinetic energy, generates energetic winds and/or jets that may surpass the galaxy's escape velocity. These feedback processes create complex interactions between stellar and SMBHs acrretion activities and the host galaxy (Springel & Hernquist 2003a,b; Schaye et al. 2010; Muratov et al. 2015). At the galactic level, these feedback processes have the capacity to raise the temperature of the ISM, inhibiting the cooling of gas and impeding the formation of stars in both small and large galaxies (Heckman et al. 2000; Bertone et al. 2007).

2.2 Virial Theorem

The virial theorem povides a general equation that relates the average total kinetic energy overtime of a stable system of discrete particles, with the gravitational potential energy of the system. The theorem mathematically states as below:

$$2\langle T\rangle + \langle U\rangle = 0 \tag{1}$$

where T is the kinetic energy and U is the gravitational potential energy of the system.

In astronomy, defining the mass and size of galaxies is challenging due to their infinite extension in continuous fluids. The virial theorem and related concepts, such as equation (1), help establish virial equilibrium. In this state, the radius is approximated as the distance where average density exceeds the critical density by a specific factor:

$$p(< r_{vir}) = \Delta_c p_{crit}(t) = \Delta_c \frac{3H(t)^2}{8\pi G} \tag{2}$$

Where H(t) is Hubble parameter, G is the gravitational constant, and factor Δ_c is called overdensity.

The virial mass is then defined relative to the radius as:

$$M_{vir} = \frac{4}{3}\pi r_{vir}^3 \Delta_c p_{crit}(t) \tag{3}$$

3 Materials and Scientific Methods

3.1 IllustrisTNG

The IllustrisTNG simulation (Nelson et al. 2021) is a suite of cosmological magnetohydrodynamical simulations of galaxy formation which present the next generation of the Illustris simulation (Genel et al. 2014; Vogelsberger et al. 2014). TNG models the galaxy formation by solving the equations of gravo-magnetohydrodynamics on the cosmological scales, generated from the moving-mesh AREPO code (Springel 2010). It includes multiphysics of radiative cooling of gas, formation of stars, stellar evolution, stellar feedback, and also supermassive blackholes feedback, aiming to predict the observational signatures of galaxies formation and evolution.

The TNG model introduced three main periodic cosmological volumes with side lengths of ~ 50 Mpc (TNG50), 100 Mpc (TNG100) and 300 Mpc (TNG300). The smallest box TNG50 has the highest resolution, while the largest box TNG300 has the lowest resolution but provides the best statistics. In this work, we used the box compromises between two limits with the highest resolution level TNG100-1, employing more than 10 billion resolution elements. We choose the simulation run at the present galaxy with z = 0.01.

In order to identify the structures such as haloes, subhaloes, and thereby galaxies, we use the Friends of Friends (FOF) algorithm (Davis et al. 1985), which groups the dark matter particles with distances smaller than linking length b = 0.2. The other types of particles (gas, stars and black holes) are assigned to the groups of nearest dark matter particles. Each group of particles is so-called a FOF halo. For each halo, we use the SUBFIND algorithm (Springel et al. 2001) to indentify the subhaloes, the gravitationally bound substructures. For each FOF halo, one central subhalo is defined, the rest of subhaloes are considered as satellite subhaloes.

According to section 2.2, we define a halo boundary by the virial radius R_{200c} representing the radius at which the galaxy's overdensity Δ_c = 200. In other words, this is the radius where total matter density inside equals 200 times the critical density of the Universe . The mass M_{200c} within this radius is considered as halo mass.

3.2 Selecting samples

In this work, we selected the haloes whose central galaxies's stellar mass $M_* > 10^9 M_\odot$ for three tasks: star formation rates, baryon mass fraction and temperature of gaseous haloes. The selected sample corresponds to haloes that harbor the central massive galaxies (see the Figure 5). With the SMBH and halo mass task, we set the threshold at $M_* > 10^6 M_\odot$ in order to capture all the phases of SMBH evolution.

3.3 Star formation rate

Each halo contains a myriad of galaxies, namely subhalos, but we are only interested in the first/central subhalo, which is usually also the most massive subhalo in the corresponding halo. Besides, detailed data for the SFR are already available for each subhalo in the IllustrisTNG. However, since we want to do the calculation ourselves in lieu, we computed it manually and cross-checked with the provided data. In order to make analysis on separated aspects, the regions to be examined the SFR are divided into 2 ranges: SFR in the 2 times half-mass radius and within a fixed physical radius of 30 kpc.

Initially, the composition of each subhalo is of great numerousness of gas cells. Therefore, for individual subhalos, we make an aggregation of the instantaneous SFR of each gas cell which is located within the predetermined radius. In addition, owing to the fact that the masses of galaxies are not constant, they may contribute significantly to the obtained SFR. Consequently, we calculate the sSFR as well, which is defined as

$$sSFR = \frac{SFR}{M_*}$$

where M_* is the stellar mass of the subhalo. By doing this, we can extract the bias for all subhalos and create a normalization among them.

Based on the $sSFR - M_*$ relation, we classify galaxies among three categories: star-forming, "green valley", and quiescent or quenched galaxies.

3.4 Baryon mass fraction

We measure the stellar mass fraction (f_s), gas mass fraction (f_g) and blackholes mass fraction (f_{bhs}) within a defined radius R (i.e. R_{200c} and 30 kpc). With each i component (gas, stars and black holes), the mass fraction is expressed as:

$$f_i = \frac{M_i}{M_{200c}}$$

where M_i is the mass of all particles of each component within a sphere of radius R, centered at the halo centre. The baryonic mass fraction is defined as the sum of all types of particles except dark matter:

$$f_b = f_g + f_s + f_{bhs} \tag{4}$$

Assuming that galaxies are cosmic "closed boxes" that retain all their baryonic matters, the predicted value of baryon mass fractions should approximately equals the cosmic baryon fraction $f_{b,cosmic}$. From the Cosmic Microwave Background (CMB) data (Planck Collaboration 2020), we obtain the cosmic baryonic fraction as:

$$f_{b,cosmic} = \frac{\Omega_b}{\Omega_b + \Omega_c} = 0.157 \pm 0.001$$

where $\Omega_b h^2 = 0.0224 \pm 0.0001$ is the baryonic density and $\Omega_c h^2 = 0.120 \pm 0.001$ is the dark matter density (h = 0.6774 × 100 km/s/Mpc is the Hubble constant).

3.5 Temperature of the gaseous haloes

To investigate the thermal properties of gaseous galaxy haloes, we calculate the mass-weighted gas temperature within the virial radius R_{200c}. The computation involves determining the temperature of each gas cell within this region and the temperature in Kelvin is given by

$$T = (\gamma - 1) \times \frac{u}{k_B} \times \frac{UnitEnergy}{UnitMass} \times \mu \tag{5}$$

Here $\mu = \frac{4}{1 + 3X_H + 4X_H x_e} \times m_p$ is the mean molecular weight, $\gamma = 5/3$ is the adiabatic index, u is the internal energy, x_e is the electron abundance, k_B is the Boltzmann constant in CGS unit, m_p is mass of proton and $X_H = 0.76$ is the hydrogen mass fraction.
The mass-weighted temperature is then defined as

$$T_{mw} = \frac{\sum(m_i * T_i)}{\sum m_i} \tag{6}$$

Where m_i and T_i are the mass and temperature of the ith gas cell.
Simultaneously, assuming that galaxies are in virial equilibrium, from the virial mass and virial radius, we can define the virial velocity and virial temperature for each galaxy's halo as:

$$V_{vir}^2 = \frac{GM}{R_{vir}} \tag{7}$$

$$T_{vir} = \frac{\mu m_p}{2k_B} V_{vir}^2 \tag{8}$$

Where μ is the mean molecular weight and k_B is the Boltzmann constant.
Then, compare the mass-weighted temperature with the virial temperature as a funciton of virial mass M_{200c}

3.6 The relationship between SMBH and halo mass

In TNG simulations, SMBH seed masses of $1.18 \times 10^6 M_\odot$ are planted when halo masses exceed $7.38 \times 10^{10} M_\odot$. Subsequently, SMBHs grow through gas accretion and galaxy merging (Weinberger et al. 2018). In return, SMBHs release feedback energy proportional to the accretion rate.

Within the TNG simulations, AGN feedback is characterized by a two-mode model. In this model, SMBHs can emit feedback energy to the surrounding environment in both thermal (thermal mode) and kinetic (kinetic mode) forms. The quantity of injected energy is dictated by the accretion rate onto the SMBH (Weinberger et al. 2017). The distinction between the two feedback modes is established by the SMBH's accretion rate; the thermal mode is active during high accretion rates, while the kinetic mode is activated at low accretion rates. Specifically, SMBHs are presumed to be in the thermal mode as long as their Bondi–Hoyle–Lyttleton accretion rate (Hoyle & Lyttleton 1939; Bondi & Hoyle 1944; Bondi 1952) exceeds a fraction χ of the Eddington accretion rate. If it falls below that threshold,

the kinetic mode is active.

$$\chi = \min\left[\chi_0 \left(\frac{M_{BH}}{10^8 M_\odot}\right)^\beta, 0.1\right] \tag{9}$$

where χ_0 and β are parameters.

While a comprehensive study of a SMBH's actual growth requires observing a galaxy's history from the inception of hosting an SMBH, our approach involves plotting the present-day masses of halos against their corresponding SMBH masses, providing a quasi-representation of SMBH growth dynamics. Within a given subhalo, it is common to find multiple supermassive black holes (SMBHs). The considered SMBH mass (M_{BH}) is specifically associated with the most massive SMBH within its host subhalo. As for the halo mass, we employ M_{200c}.

To examine the scaling relations between the supermassive black hole (SMBH) and halo mass, the data undergoes fitting to a single power law in logarithmic space through linear least-squares regression. We also quantify the correlation significance between the two masses using the Pearson correlation coefficient (r_P). Furthermore, we consider the associated p-value for assessing non-correlation. As a reference, correlations with absolute values within the ranges [0.8, 1.0], [0.5, 0.8], [0.3, 0.5], or [0.0, 0.3] are generally categorized as strong, moderate, weak, or nonexistent, respectively. The chosen threshold significance level is set at $p = 0.05$, where $p < 0.05$ indicates that the data is unlikely under the null hypothesis.

4 Results

4.1 Star formation rates

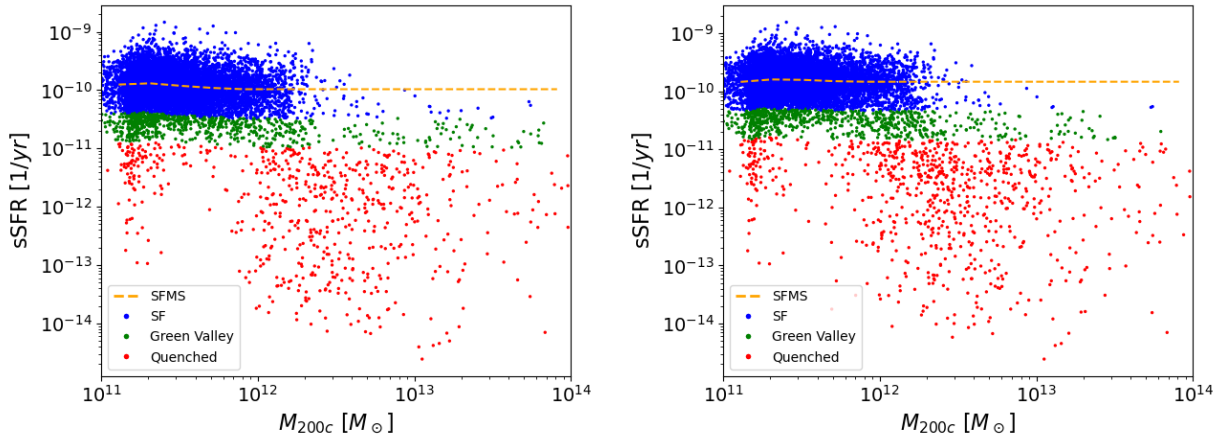

Figure 1: sSFR vs. M_{200c} within 2 times half-mass radius (left) and within a fixed physical radius of 30kpc (right). The orange dashed line represents the star-forming main sequence (SFMS). The blue solid circles show the star-forming galaxies (SF). The green solid circles illustrate the green valley galaxies while the black ones symbolize the quenched (quiescent) galaxies.

Firstly, we visualize the distribution of sSFR with M_{200c} and evaluate the median relation between them. Then, we noticed that galaxies in the range from $10^{11} M_\odot$ to $10^{12} M_\odot$ are densely populated. Hence, we use a bin mass of 0.2-dex when searching for the median relation to approximate the star-forming main sequence (SFMS). For those galaxies whose logarithmic distance ($\log \Delta_{sSFR}$) exceeds -0.5 dex from the SFMS at their respective mass, we designate them as star-forming galaxies. Next, they are used to approximate the SFMS one more time to make sure the SFMS for each approximation converges and creates consistency during the process. For galaxies with M_{200c} surpasses $10^{12} M_\odot$, the SFMS is linearly extrapolated. As soon as the SFMS is constructed, the "green valley" ($-1.0 < \log \Delta_{sSFR} < -0.5$) and quenched ($\log \Delta_{sSFR} < -1.0$) galaxies could be specified based on their logarithmic distance at their specific mass (Pillepich et al. 2019).

From Figure 1, the population of galaxies is similar across the mass range in both cases of the radius. Star-forming galaxies concentrate mostly in the range from $10^{11} M_\odot$ to $10^{12} M_\odot$. Although "green valley" and quenched galaxies are also present in the mediate-mass region, their distribution increases dramatically in the massive-mass region while there is a drop in the number of star-forming galaxies.

4.2 Baryon mass fraction

Figure 2 shows the contribution of each component in virial radius R_{200c} and the stellar component in the observable galaxy disk of 30 kpc in radius as the function of M_{200c}. Overall, almost all haloes in TNG simulations have a baryon fraction lower than the cosmic value within their boundary, except for very few haloes in range 10^{11} to 10^{12} $M_\odot$ (referred to

Figure 8e). Most of the baryon fraction is contributed from gas fraction, except for the region where $M_{200c} \lesssim 6 \times 10^{10}\ M_\odot$ where the number of sample is small, leading to the high uncertainty when estimating the median. We can quantify some behaviors of mass fraction into 3 regions:

- *Low-mass haloes* ($10^{11} M_\odot \lesssim M_{200c} \lesssim 10^{12} M_\odot$): The majority of baryon fraction is from the gas fraction and a small amount of stellar fraction. In this range, nearly all the stellar masses reside in the radius 30 kpc.
- *Milky Way to group-mass haloes* ($10^{12} M_\odot \lesssim M_{200c} \lesssim 10^{14} M_\odot$): At about $2 \times 10^{12} M_\odot$ the gas and stellar fraction are nearly the same. Then gas fraction increases significantly while the stellar fraction decreases gradually. Stellar masses of haloes mostly fall outside of radius 30 kpc.
- *Galaxy clusters* ($M_{200c} \gtrsim 10^{14} M_\odot$): The baryon fraction nearly reach the cosmic value and level off at ~ 0.15.

Note that we do not demonstrate the mass fraction of black holes because it is too small compared with other components (referred to Figure 8d).

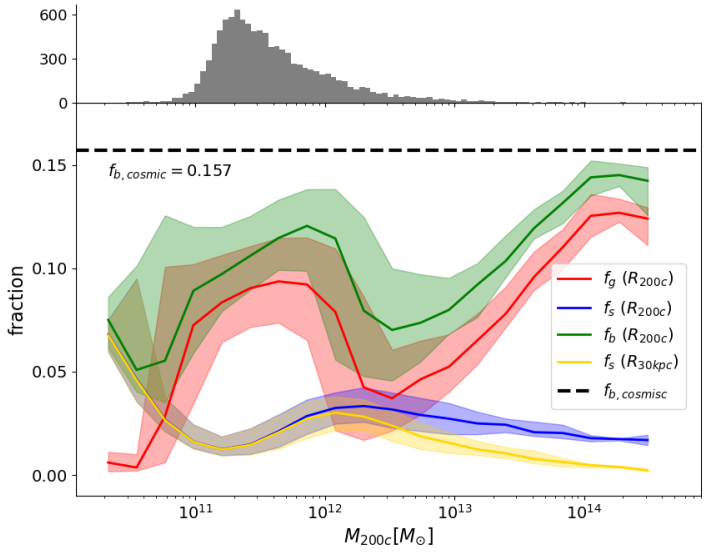

Figure 2: The relation between the halo mass and halo gas, stars and baryon fraction within R_{200c} and stars fraction within 30 kpc. Colored lines represent the median of mass fraction of each components. Shaded areas represent the 16^{th} to 84^{th} percentile. Dashed line shows the observational cosmic baryonic fraction. *Top panel:* The histogram of M_{200c}. The majority of the selected sample's mass falls within 10^{11} to 10^{14} $M_\odot$

4.3 Temperature of the gaseous haloes

Figure 3 illustrates the relationship between the virial temperature of 7651 primary galaxies' haloes and their mass-weighted temperature T_{mw} concerning virial mass. Notably, the

trend of T_{mw} appears to exhibit a nearly linear behavior, particularly evident for galaxies with masses exceeding 1.3×10^{11} solar masses. Intriguingly, the computed mass-weighted temperature consistently registers as lower than the prediction derived from the virial theorem, and there is a noticeable convergence between them at the high mass end.

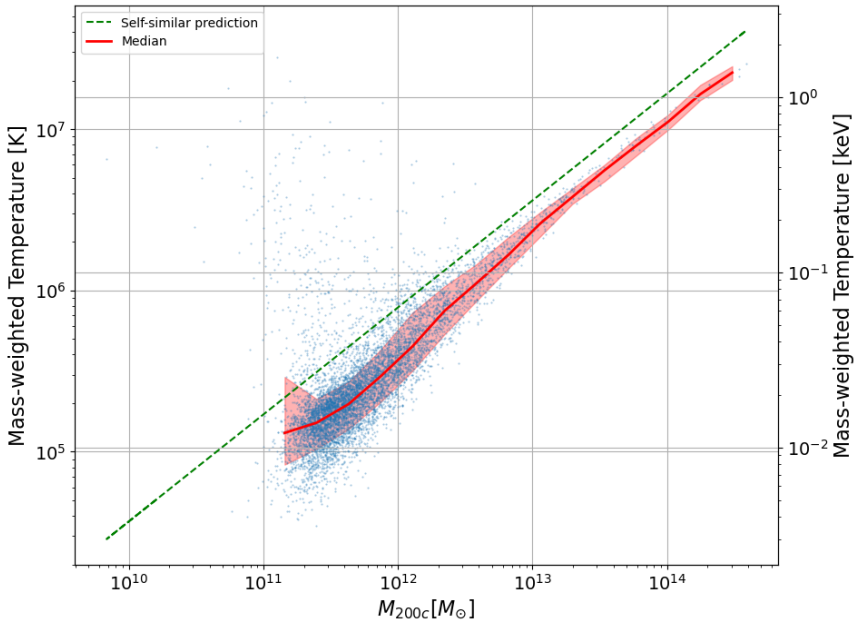

Figure 3: Comparison between T_{vir} vs M_{200c} and T_{mw} vs M_{200c}. The data points represent the mass-weighted temperature of each galaxies. The red line represents the median value of the galaxies' temperature as a function of M_{200c}. The green dashed line is the relation between virial temperature of galaxies and their virial mass.

Additionally, there are some data points with unusually high temperatures at low masses, which we consider outliers (referred from Figure 6). To ensure a more accurate analysis, we choose to remove the median value in this mass range, helping to improve the reliability of the relationship between mass-weighted temperature and virial mass.

4.4 The relationship between SMBH and halo mass

Figure 4 displayed the relationship between black hole mass (M_{BH}) and halo mass (M_{200c}) for the TNG100-1 galaxy sample at redshift $z = 0.01$, comprising 25,244 halos where $M_{BH} > 0$. The M200c histogram indicates a peak concentration within the range of $10^{11}M_\odot < M_{200c} < 10^{12}M_\odot$. Both the MBH and M200c histograms exhibit a decreasing scatter as the mass increases.

From Figure 4, assuming that the SMBH growth in time can be approximated by the $M_{BH} - M_{200c}$ scaling relation at $z = 0.01$, it can be categorized into 3 phases:

- *First phase* ($M_{200c} \lesssim 10^{11}M_\odot$): The growth of SMBH mass is negligible.
- *Second phase* ($10^{11}M_\odot \lesssim M_{200c} \lesssim 10^{12}M_\odot$): SMBH mass exhibits a power-law increase - $M_{BH} \propto M_{200c}^{0.74}$.

- *Third phase* ($M_{200c} \gtrsim 10^{12} M_\odot$): As the halo mass approaches that of the Milky Way, SMBH growth rate starts to diminish - - $M_{BH} \propto M_{200c}^{0.73}$.

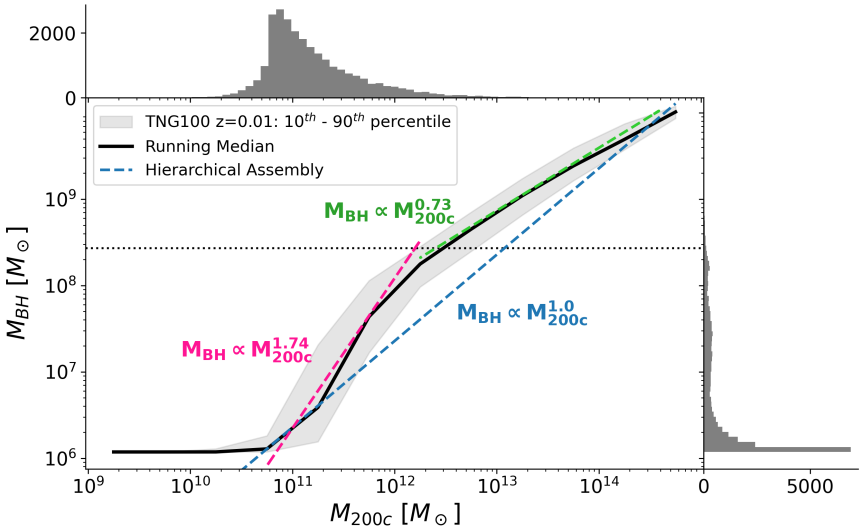

Figure 4: *Main panel:* SMBH mass vs. halo mass for the galaxy sample with $M_* > 10^6 M_\odot$ at $z = 0.01$. The pink and green dashed lines are best fit lines showing the data's slopes in the second and third phases, while the blue dashed line shows the SMBH - halo mass scaling relation by the hierarchical assembly through galaxy merging. The solid black line represents the running median for the sample. The horizontal dotted line shows the approximate SMBH mass where the second phase of SMBH growth transitions to the third phase. *Sub panel:* Histograms of M_{BH} and M_{200c}

Table 1: Pearson Correlation Coefficients, Standard Errors and p-values for the three phases

	First phase	Second phase	Third phase
r_P	0.020	0.889	0.908
SE_r	0.021	0.003	0.014
p-value	0.356	0.00	0.00

Table 1 shows the results of the Pearson correlation coefficient calculations. Notably, there are high correlation coefficients r_P and very low p-values (p-value $\simeq 0.0$) in the second and third phases. The standard error SE_r is lowest in the second phase due to its large population size.

5 Discussion

5.1 Star formation rate

Within the mass range of $10^{11} - 10^{12} M_{\odot}$, galaxies exhibit robust star formation activities. This range represents a critical transitional phase where gravitational interactions, gas accretion, and other dynamic processes drive the formation of new stars. To delve into the details, galaxies take energy from supernovae so the intergalactic medium (IGM) is a region of hot, ionized gas and the SMBH feedback is supposed to be an agency of star formation quenching in TNG central massive galaxies. Particularly, they redistribute the gas out of the inner regions into a larger scale while simultaneously heating up the medium, expand its cooling times, and by that means intercepting the progenitors of future star formation (Truong 2020).

"Green valley" highlights the discriminating power of UV to very low relative levels of ongoing star formation and it relates to those below the star-forming main sequence (Salim 2014). Although their population is already distributed across the mass range, as galaxies evolve, a noticeable event occurs in the transition from active star-forming galaxies to those in the region of "green valley". Therefore, in the region above $10^{12} M_{\odot}$, it is witnessed a noteworthy decrease in the population of star-forming galaxies. This decrease demonstrates the intricate relationship that exists between SMBHs and the gas reservoirs that support star formation.

Above the mass scale $M_{200c} \sim 10^{12} M_{\odot}$, which is approximately the Milky Way's mass, there is a prevalence of quenched galaxies. The accreting mass of SMBHs in these high-mass galaxies makes them aggressively active and correlates with a more efficient regulation of the gas supply, diminishing almost the star-forming process in galaxies. This leads to the domination of quenched galaxies in the higher mass range.

5.2 Baryon mass fraction

In the ΛCDM model, the hierarchical structure formation of the Universe suggests that dark matter haloes forms the potential wells that baryons fall into. The baryonic matter starts off as gas which interacts mostly via heating and cooling processes. Gravity collapses the gas forming complex structures like stars and galaxies. The stars feedback to the cosmic baryon cycle by radiating energy and ejecting heavy elements into interstellar medium. All the processes are considered to happen within each the dark matter halo, leading to the fact that baryons and dark matter should be coupled with baryon fraction f_b close to the observational cosmic value ~ 16%.

However, many observations from the X-ray and Sunyaev Zel'dovich (SZ) surveys (e.g. Gonzalez et al. 2013; Eckert et al. 2021) report that haloes may not contain all their associated baryons within virial radius R_{200c}, which often referred to as the missing baryons problem. Our results in section 4.2 agree with the previous findings and can be understood by considering some critical physical processes such as stellar and AGN feedback (Ayromlou et al. 2023).

For the low-mass haloes region ($10^{11} M_\odot \lesssim M_{200c} \lesssim 10^{12} M_\odot$), the dominant physical processes affect the baryon fraction is stellar feedback. This process can eject the interstellar gas into circumgalactic medium which results in the large proportion of gas fraction in this region. The analysis of star formation rates in section 5.1 support this argument because the star formation rates in this region is extremely high.

For group-mass haloes ($10^{12} M_\odot \lesssim M_{200c} \lesssim 10^{14} M_\odot$) region, AGN feedback is the main driving force in redistributing the baryon mass fraction within the virial radius by pushing the gas from the inner halo to outskirt regions. This was justified by the significant decreases in the star formation rates and the third-phase (kinetic feedback phase) entering of SMBHs (see more in section 5.4). This scenario leads to the fact that the baryon fraction f_b is about half of the cosmic value $f_{b,cosmic}$ in this region.

For galaxy clusters ($M_{200c} \gtrsim 10^{14} M_\odot$) region, the deep gravitational potential wells prevent the efficient gas ejection beyond the halo boundary, so the baryon fractions in most massive clusters are very close to the cosmic baryon fraction.

5.3 Temperature of gaseous haloes

As shown in Figure 3, the green dashed line emphasized the relation in equation (8): correlations between thermal properties of gas and total mass of halo in the absence of SMBHs and their feedback with the assumption that the galactic system is in virial equilibrium. Thus, the gas temperature is chiefly driven by the halo mass according to the virial theorem.

On the other hand, the result of T_{mw} shows a strong and tight increasing relation between thermal properties of gas and total mass of halo around galaxies, even though these galactic system take into account the presence of complex astrophysical phenomenon such as stellar feedback and SMBH feedback. However, the slope of this relation do have some different from the self-similar prediction of section 2.2 but it get smaller when it comes to high-mass end.

The gas accretion triggers SMBH feedback which, in turn, affects the thermodynamic and density properties of gaseous atmosphere. In the context of massive, quenched galaxies in section 5.1, this feedback raise the temperature of the gaseous halo (Davies et al. 2019). On the other hand, Fig.3 shows that the calculated mass-weighted temperature of the haloes is lower than the prediction, indicating a potential cooling effect on the them.

Furthermore, as discussed in Section 4.3, data points with exceptionally high temperatures but low masses are identified as outliers, given their rarity. This can be attributed to the influence of small galaxies, where the thermal effects of SMBH feedback and stellar feedback, like supernovae, significantly impact the gas's thermal properties in the halo. As the total halo mass increases, the feedback from stars and SMBHs becomes less significant, potentially explaining the convergence between T_{vir} and T_{mw} at high mass end.

5.4 The relationship between SMBH and halo mass

From Figure 4, the growth of SMBHs in IllustrisTNG simulations unfolds in three distinct phases. Initially, as described in 3.6, the SMBH seed masses of $\sim 10^6 M_\odot$ are planted, hence we can see that the minimum SMBH mass M_{BH} is approximately the same as this seeding mass. Furthermore, in the low-mass range (equivalent to early stages), the growth of SMBHs is minimal due to stellar feedback. This influence hinders the growth of SMBHs in galaxies with a total halo mass less than $10^{11} M_\odot$. In the absence of stellar feedback, low-mass galaxies can experience more effective SMBH growth even prior to reaching a halo mass of $10^{12} M_\odot$.

In the second phase, SMBHs experience accelerated expansion when they attain a mass at which gravitational forces counteract stellar feedback. Radiative cooling contributes to this growth by preventing the excessive expulsion of gas. Essentially, the hot atmospheres lead to an increase in accretion rates, the radiative cooling rates would then be larger and the flow becomes cooler, preventing the gas from reaching extreme temperatures where it would be more prone to expulsion (Dihingia et al. 2023). Consequently, in this phase, potentially due to the formation of hot atmospheres, SMBHs can undergo rapid expansion through the accretion of (cold) gas. Throughout this period, the pace of SMBH growth is governed by the depth of the galaxy's gravitational potential well, ensuring that SMBHs cannot undergo excessively rapid growth, as this would disrupt the accretion flows due to their feedback (Terrazas et al. 2020; Booth & Schaye 2010).

The third phase sees a decline in the SMBH growth rate, transitioning from thermal to kinetic feedback. In the process of heating up the surrounding gas, the kinetic feedback also efficiently expels gas from the SMBH's vicinity, thus increases its cooling time, limiting further star formation (Weinberger et al. 2018; Davies et al. 2020; Terrazas et al. 2020). SMBH growth is self-regulated through kinetic feedback, preventing excessive gas accretion and maintaining a relatively small scatter in the correlation between SMBH mass and total halo mass. The presence of a SMBH - halo mass scaling relation is consistent with the hierarchical assembly of large-scale structures (Jahnke & Macciò 2011). Despite a deviation from a linear relationship ($M_{BH} \propto M_{200c}^{1.0}$) in the third phase, which may be attributed to extra mass gained through gas accretion in the second phase, the dominant role of mergers in SMBH growth persists.

Additionally, from Table 1, we note that the Pearson correlation coefficient is the highest in the third phase, with $r_P \simeq 0.908$ and p-value $\simeq 0.0$, implying strong correlation between M_{BH} and M_{200c} in the regime $M_{200c} \gtrsim 10^{12} M_\odot$. On the other hand, the low correlation coefficient $r_P \simeq 0.02$ and p-value $\simeq 0.356 > 0.05$ reflect the fact that the SMBHs hardly grow in the first phase.

6 Summary and Conclusions

(i) The study of the correlation between sSFR and M_{200c} in the crowded region of 10^{11} – $10^{12} M_{\odot}$ has revealed an interesting story of galaxy evolution. The dense population seen in this mass range indicates a dynamic stage of star formation, implying a favorable environment for star birth. But the threshold of $10^{12} M_{\odot}$, a key shift occurs that signals a turning point in the history of galaxies: star formation declines, the green valley and quenched galaxies dominate.

(ii) We have discovered a relation between the baryon mass fraction within the virial radius and the halo mass. The majority of the baryon mass comprises gas, with a minor contribution from stellar mass. We also discussed the dominant physical processes impacting the distribution of baryons. Stellar feedback dominates in the low-mass halo region ($10^{11} M_{\odot} \lesssim M_{200c} \lesssim 10^{12} M_{\odot}$), leading to an increase in the gas fraction. AGN feedback dominates in the group-mass halo region ($10^{12} M_{\odot} \lesssim M_{200c} \lesssim 10^{14} M_{\odot}$), ejecting gas beyond the halo boundary and reducing the baryon fraction. Galaxy clusters ($M_{200c} \gtrsim 10^{14} M_{\odot}$) are the least affected by astrophysical processes and typically retain most of their baryons within the virial radius R_{200c}.

(iii) We explored the connection between the temperature and the overall mass of galactic halos, contrasting it with the self-similar forecast derived from the virial theorem. For halos with $M_{200c} > 1.3 \times 10^1 1 M_{\odot}$, their thermal characteristics exhibit a comparable trend to the theoretical prediction. Despite some differences between the calculated and predicted values, the halo temperature converges towards the prediction with an increase in halo mass. This convergence is attributed to the diminishing significance of feedback from stars and SMBHs in massive galaxies. The observation that the mass-weighted temperature of the halo is lower than the prediction suggests a potential cooling effect on the halo.

(iv) In TNG simulations, the evolution of SMBHs can be broadly categorized into three distinct phases (refer to Figure 4): an initial stage of slow or negligible growth in low-mass galaxies ($M_{200c} \lesssim 10^{11} M_{\odot}$), primarily influenced by stellar feedback that restrains the accumulation of significant amounts of dense gas in the galactic center; a subsequent period of rapid growth in intermediate-mass galaxies ($10^{11} M_{\odot} \lesssim M_{200c} \lesssim 10^{12} M_{\odot}$) driven by gas accretion; and a subsequent decline in massive galaxies ($M_{200c} \gtrsim 10^{12} M_{\odot}$), where SMBH feedback induces heating and expulsion of gas from the galactic center, and SMBHs predominantly grow through mergers. In the third phase, there is a strong correlation ($r_P \simeq 0.908$ and p-value $\simeq 0.0$) between SMBH masses and the masses of their host halos, a pattern that may naturally arise from the hierarchical assembly process.

In conclusion, it is inferred that in the mediate-mass range of the galaxies between 10^{11} – $10^{12} M_{\odot}$, SMBH is not very active, allowing the intergalactic space to cool down, appropriate for giving birth to stars and contributing to the distribution of gas in the halos. However, because SMBHs co-evolve with galaxies, in the massive area above $10^{12} M_{\odot}$, SMBHs grow huge and active, heating up the medium and expelling gas from the galaxies, preventing star formation.

7 Management of the project

This section provides an evaluation of the accomplishments in comparison to the initial plan. While we adhered to the plan to the best of our ability, unforeseen challenges arose during the project, as outlined in Table 2. Challenges arose due to our limited experience with the IllutrisTNG simulation. On a positive note, we stuck to the deadlines for each phase, avoiding significant delays. The team members demonstrated good self-discipline in their work.

Table 2: Management Plan

Plan	**Done**	**Cause of the difference**
Overview of IllutrisTNG Simulation	Finished the overview	None
Examing the relationship between mass of galaxy (M_*), M_*/M_{tot} against M_{tot} of subhalos	We found a linear distribution of M_* and M_*/M_{tot} against M_{tot} of subhalos at $M_* > 10^{10}$ solar mass	We successfully completed the analysis without any problems
• Measure the f*, f_g within R_{200c}. Plot f*, f_g and $f_b = f* + f_g$ as a function of M_{200c}. • Compute the M_{BH} within the M_{200c}. • Measure and plot the T_mw within R_{200c}. • Measure the SFR within 2 times half-mass radius and a fixed radius of 30 kpc and create plots of SFR-M* and sSFR-M*.	• We found the relation of gas, stellar and baryon fraction with halo mass. • We found three distinct phases of M_{BH} growth. • We found a sort of linear distribution of T_{mw} against M_{200c} when $M_{200c} > 1.3^{11}$ solar mass. • We found a distribution of galaxies in different star-forming stages across all the mass ranges. A similarity can be seen between 2 radii of interest.	• None • None • None • None

Plan	Done	Cause of the difference
• Investigate the predicted value of baryonic fraction in case galaxies are cosmic "closed boxes" that retain all their baryonic matter. • Study the expected M_{BH} – M_{200c} relation based on hierarchical assembly in SMBHs and host galaxies. • Calculate the virial temperature as a function of M_{200c} assuming galaxies are in virial equilibrium. • Define the SFMS, star-forming, "green valley", and quiescent galaxies.	• The distribution of baryon mass fraction hugely affected by the stellar and black holes feedback. • The expected M_{BH} – M_{200c} relation would be $M_{BH} \propto M_{200c}^{1.0}$. • We found that the calculated T_{mw} is a bit lower than self-similar prediction from virial theorem. The mass-weighted temperture and virial temperature converge when it comes to high mass end. • The star-forming galaxies thickly occupy in 10^{11} – $10^{12} M_{\odot}$ with the SFMS running across them. The green valley and quenched galaxies spread out the mass ranges with a dominance beyond $10^{12} M_{\odot}$.	• It would be better if we are able to run some fiducial TNG simulations (Pillepich et al. 2018) without stellar feedback or AGN feedback to directly confirm our findings. • None • We could not perform calculation on cooling rate because the snapshot we used does not support this. • None
Attend the lectures on related topic	Done	None
Cross-checking, discuss, evaluate, interpret the obtained results, and complete the report	Finished	None

As for our individual work, there have been modifications to how each of the group members will carry out their designated parts. For most of the time other group members will act as overseers to monitor the situation and progress of one's work, and also involve themselves for assistance if necessary. The following list depicts our original missions assigned, how

every member handled it and cooperated with the rest:

1. Nguyen Thi Yen Binh: She is tasked with examining the connection between baryon mass fraction within the virial radius to identify the primary physical processes influencing the distribution of baryons.

2. Trinh Hoang Dieu Ngan: She is responsible for examining the relationship between SMBH and halo mass, aiming to unravel the evolution of SMBH corresponding to different halo masses.

3. Nguyen Phu Huy: He is assigned to explored the connection between the temperature and the total mass of the halo, from then investigate the SMBH feedback on the thermal properties of gas in the halo.

4. Huynh Quoc Thang: He is assigned to explore the correlation between sSFR and halo mass, delving into the dynamics of star formation to unveil the environmental conditions of galaxies and their evolution.

References

Ayromlou, M., Nelson, D., & Pillepich, A. 2023, Monthly Notices of the Royal Astronomical Society, 524, 5391–5410

Bertone, S., De Lucia, G., & Thomas, P. 2007, Monthly Notices of the Royal Astronomical Society, 379, 1143

Bondi, H. 1952, Monthly Notices of the Royal Astronomical Society, 112, 195

Bondi, H. & Hoyle, F. 1944, , 104, 273

Booth, C. M. & Schaye, J. 2010, , 405, L1

Chiaki, G., Yoshida, N., & Hirano, S. 2016, Monthly Notices of the Royal Astronomical Society, 463, 2781

Davies, J. J., Crain, R. A., Oppenheimer, B. D., & Schaye, J. 2019, Monthly Notices of the Royal Astronomical Society, 491, 4462

Davies, J. J., Crain, R. A., Oppenheimer, B. D., & Schaye, J. 2020, , 491, 4462

Davis, M., Efstathiou, G., Frenk, C. S., & White, S. D. M. 1985, , 292, 371

Dihingia, I. K., Mizuno, Y., Fromm, C. M., & Younsi, Z. 2023, Impact of radiative cooling on the magnetised geometrically thin accretion disk around Kerr black hole

Eckert, D., Gaspari, M., Gastaldello, F., Le Brun, A. M. C., & O'Sullivan, E. 2021, Universe, 7, 142

Genel, S., Vogelsberger, M., Springel, V., et al. 2014, Monthly Notices of the Royal Astronomical Society, 445, 175–200

Gonzalez, A. H., Sivanandam, S., Zabludoff, A. I., & Zaritsky, D. 2013, The Astrophysical Journal, 778, 14

Heckman, T., Lehnert, M., Strickland, D., & Armus, L. 2000, Astrophysical Journal Supplement Series, 129, 493

Hoyle, F. & Lyttleton, R. A. 1939, Proceedings of the Cambridge Philosophical Society, 35, 405

Jahnke, K. & Macciò, A. V. 2011, , 734, 92

Kormendy, J. & Ho, L. C. 2013, Annual Review of Astronomy and Astrophysics, 51, 511–653

Muratov, A., Keres, D., Faucher-Giguere, C.-A., et al. 2015, Monthly Notices of the Royal Astronomical Society, 454, 2691

Nelson, D., Springel, V., Pillepich, A., et al. 2021, The IllustrisTNG Simulations: Public Data Release

Pillepich, A., Nelson, D., Springel, V., et al. 2019, Monthly Notices of the Royal Astronomical Society, 490, 3196–3233

Pillepich, A., Springel, V., Nelson, D., et al. 2018, , 473, 4077

Planck Collaboration, Aghanim, N., Akrami, Y., et al. 2020, , 641, A6

Saglia, R. P., Opitsch, M., Erwin, P., et al. 2016, , 818, 47

Salim, S. 2014, Serbian Astronomical Journal, 1–14

Schaye, J., Dalla Vecchia, C., & Booth, C. 2010, Monthly Notices of the Royal Astronomical Society, 402, 1536

Springel, V. 2010, , 401, 791

Springel, V. & Hernquist, L. 2003a, Monthly Notices of the Royal Astronomical Society, 339, 289

Springel, V. & Hernquist, L. 2003b, Monthly Notices of the Royal Astronomical Society, 339, 312

Springel, V., White, S. D. M., Tormen, G., & Kauffmann, G. 2001, , 328, 726

Terrazas, B. A., Bell, E. F., Pillepich, A., et al. 2020, , 493, 1888

Truong, N., P. A. W. N. 2020, Monthly Notices of the Royal Astronomical Society, 501, 2210–2230

Vogelsberger, M., Genel, S., Springel, V., et al. 2014, , 444, 1518

Vogelsberger, M., Marinacci, F., Torrey, P., & Puchwein, E. 2019, Cosmological Simulations of Galaxy Formation

Weinberger, R., Springel, V., Hernquist, L., et al. 2017, Simulating galaxy formation with black hole driven thermal and kinetic feedback

Weinberger, R., Springel, V., Pakmor, R., et al. 2018, Supermassive black holes and their feedback effects in the IllustrisTNG simulation

8 Appendix

8.1 Selected Samples

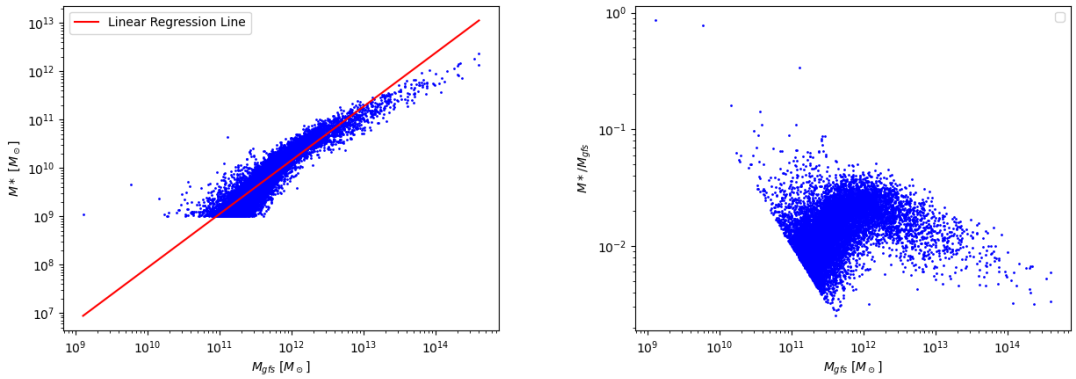

(a) Relation between stellar mass and central subhalo mass

(b) Relation between specific stellar mass with central subhalo mass

Figure 5: The selected sample with $M_* > 10^9 M_\odot$

8.2 Temperature

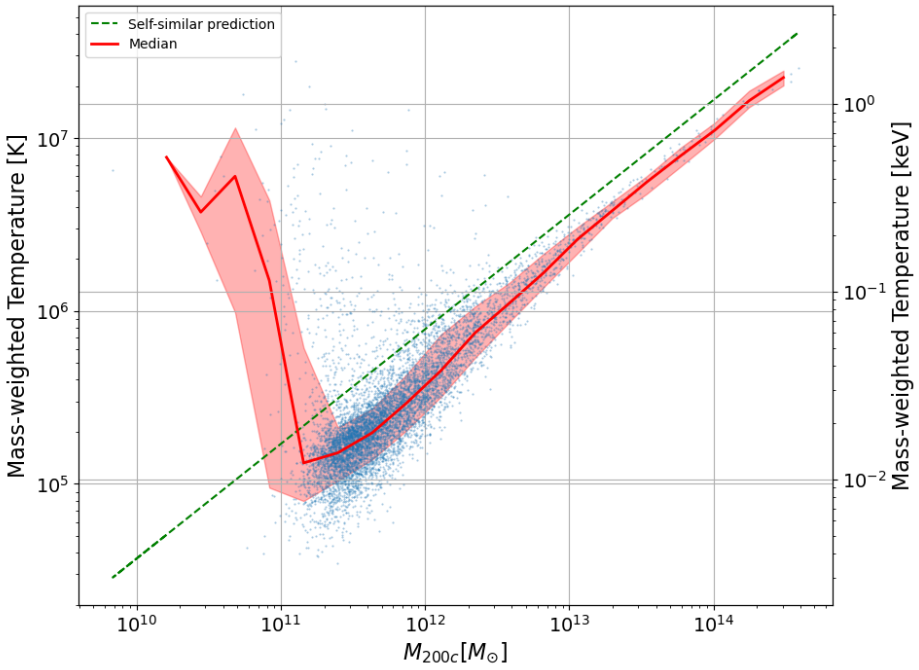

Figure 6: T_{vir} vs M_{200c} and T_{mw} vs M_{200c} with full median value of T_{mw}

Figure 7: Caption

8.3 Mass fraction

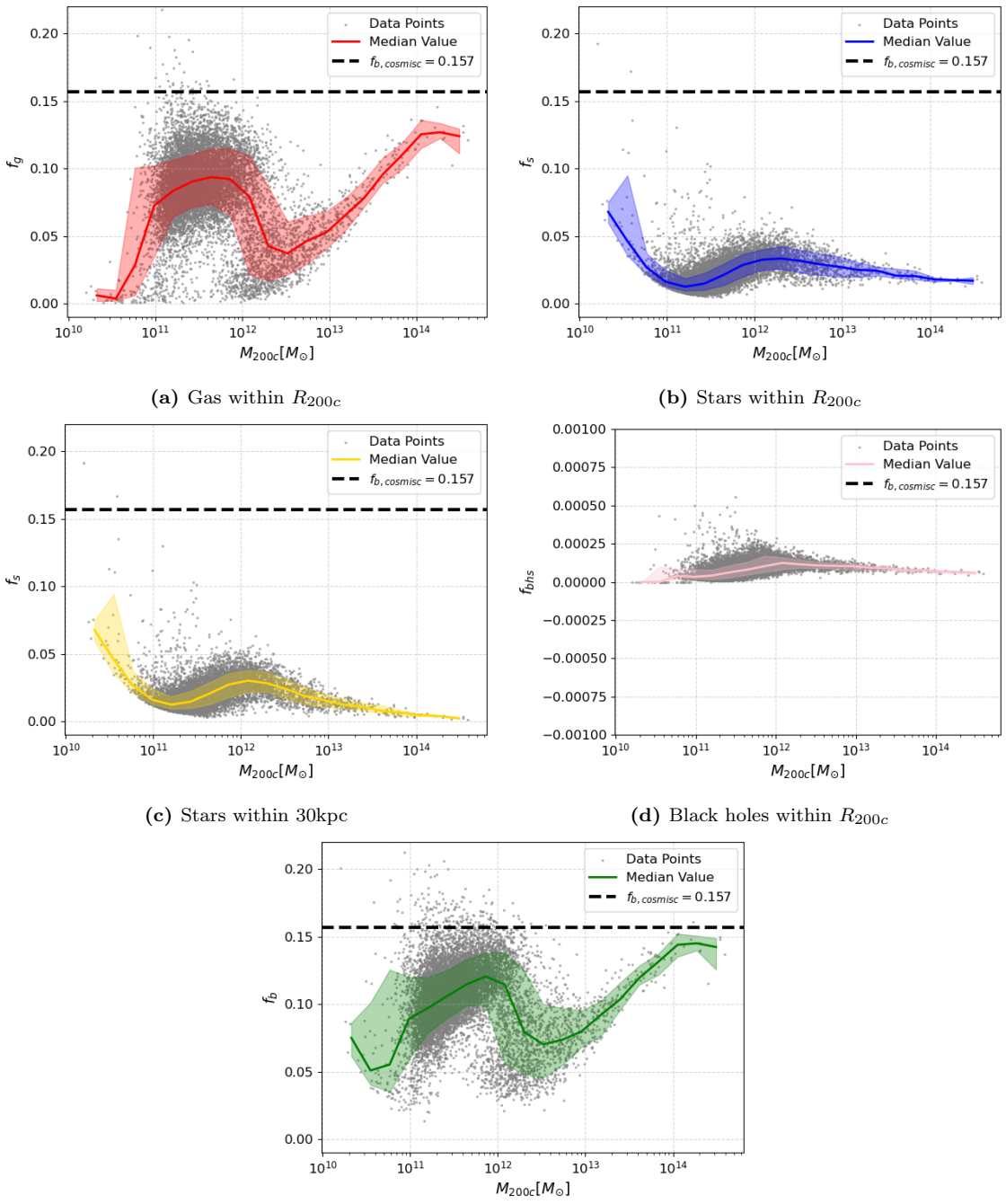

(a) Gas within R_{200c}

(b) Stars within R_{200c}

(c) Stars within 30kpc

(d) Black holes within R_{200c}

(e) Baryon within R_{200c}

Figure 8: Scatter plots and running median of mass fraction of gas, stars, black holes and baryon components

8.4 Star formation rate

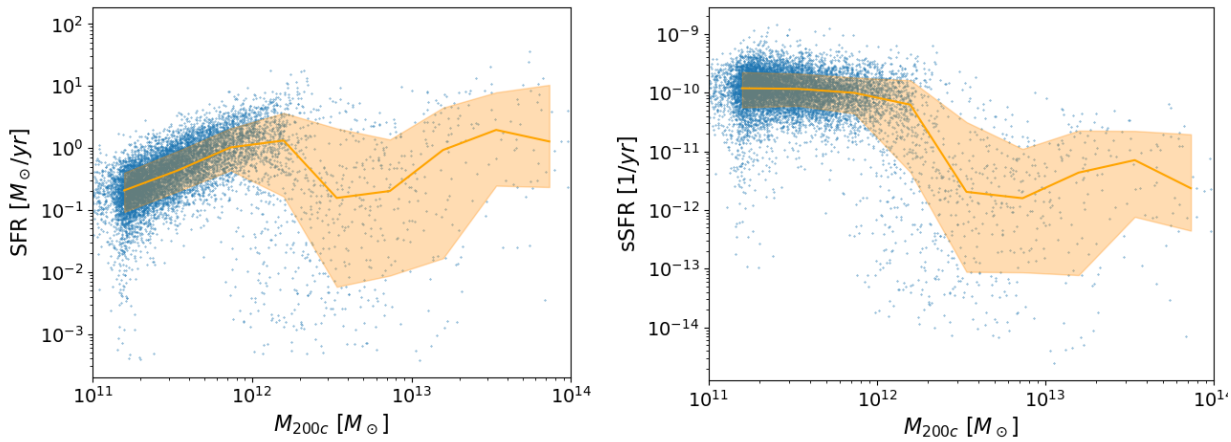

Figure 9: SFR (left) and sSFR (right) vs. M_{200c} within 2 times half-mass radius

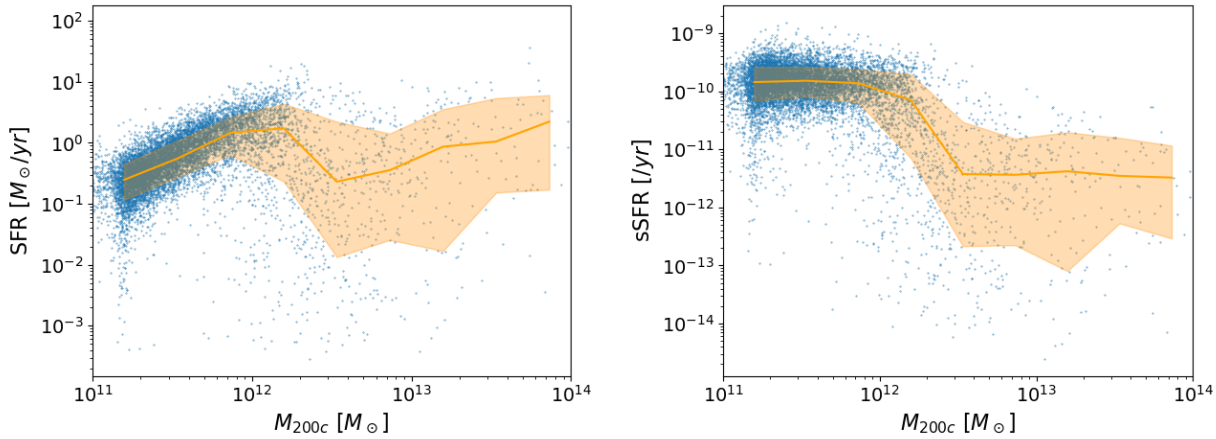

Figure 10: SFR (left) and sSFR (right) vs. M_{200c} within a fixed physical radius of 30kpc